Histotripsy for the Treatment of Cholangiocarcinoma Liver Tumors: *In Vivo* Feasibility and *Ex Vivo* Dosimetry Study

Alissa Hendricks-Wenger,

Department of Biomedical Engineering and Mechanics, Virginia Tech, Blacksburg, VA 24061 USA, also with the Department of Biomedical Sciences and Pathobiology, Virginia-Maryland College of Veterinary Medicine, Blacksburg, VA 24061 USA, and also with the Graduate Program in Translational Biology, Medicine and Health, Virginia Tech, Roanoke, VA 24016 USA

Peter Weber,

Virginia Tech Carilion School of Medicine, Roanoke, VA 24016 USA

Alex Simon,

Department of Biomedical Engineering and Mechanics, Virginia Tech, Blacksburg, VA 24061 USA

Sofie Saunier,

Department of Biological Systems Engineering, Virginia Tech, Blacksburg, VA 24061 USA

Sheryl Coutermarsh-Ott,

Department of Biomedical Sciences and Pathobiology, Virginia-Maryland College of Veterinary Medicine, Blacksburg, VA 24061 USA

Douglas Grider,

Department of Basic Science Education, Virginia Tech Carilion School of Medicine, Roanoke, VA 24016 USA, and also with Dominion Pathology Associates, Roanoke, VA 24016 USA

Joan Vidal-Jové,

Institute Khuab for Interventional Oncology, Comprehensive Tumor Center Barcelona, 08023 Barcelona, Spain

Irving Coy Allen,

Department of Biomedical Sciences and Pathobiology, Virginia-Maryland College of Veterinary Medicine, Blacksburg, VA 24061 USA, also with the Graduate Program in Translational Biology, Medicine and Health, Virginia Tech, Roanoke, VA 24016 USA, and also with the Department of Basic Science Education, Virginia Tech Carilion School of Medicine, Roanoke, VA 24016 USA

David Luyimbazi,

Virginia Tech Carilion School of Medicine, Roanoke, VA 24016 USA, and also with the Department of Surgery, Carilion Clinic, Roanoke, VA 24016 USA

Eli Vlaisavljevich

Corresponding author: Eli Vlaisavljevich. eliv@vt.edu.

Department of Biomedical Engineering and Mechanics, Virginia Tech, Blacksburg, VA 24061 USA, and also with the Graduate Program in Translational Biology, Medicine and Health, Virginia Tech, Roanoke, VA 24016 USA

Abstract

Histotripsy is a noninvasive, nonionizing, and nonthermal focused ultrasound ablation method that is currently being developed for the treatment of liver cancer. Promisingly, histotripsy has been shown for ablating primary [hepatocellular carcinoma (HCC)] and metastatic [colorectal liver metastasis (CLM)] liver tumors in preclinical and early clinical studies. The feasibility of treating cholangiocarcinoma (CC), a less common primary liver tumor that arises from the bile ducts, has not been explored previously. Given that prior work has established that histotripsy susceptibility is based on tissue mechanical properties, there is a need to explore histotripsy as a treatment for CC due to its dense fibrotic stromal components. In this work, we first investigated the feasibility of histotripsy for ablating CC tumors *in vivo* in a patient-derived xenograft mouse model. The results showed that histotripsy could generate CC tumor ablation using a 1-MHz small animal histotripsy system with treatment doses of 250, 500, and 1000 pulses/point. The second set of experiments compared the histotripsy doses required to ablate CC tumors to HCC and CLM tumors *ex vivo*. For this, human tumor samples were harvested after surgery and treated *ex vivo* with a 700-kHz clinical histotripsy transducer. Results demonstrated that significantly higher treatment doses were required to ablate CC and CLM tumors compared to HCC, with the highest treatment dose required for CC tumors. Overall, the results of this study suggest that histotripsy has the potential to be used for the ablation of CC tumors while also highlighting the need for tumor-specific treatment strategies.

Keywords

I. Introduction

MORE than 800 000 people are diagnosed with a malignancy originating from or metastatic to the liver every year. Of these, 42 810 cases are projected for the U.S. in 2020 [1]. These malignant liver tumors include hepatocellular carcinoma (HCC), liver metastasis (LM), and cholangiocarcinoma (CC). Although surgical resection remains the mainstay of liver tumor intervention, less than 25% of patients are candidates for resection due to tumor burden, location, or comorbid disease [2], [3]. For example, a prior study found that only 15% of intrahepatic CC tumors and 56% of distal tumors were deemed resectable [4].

Minimally invasive ablation methods have shown some success in treating liver tumors but have limitations due to the thermal mechanism, including lack of precision and high complication rates when treating near critical structures [5]–[14]. Histotripsy is a noninvasive, nonthermal, and image-guided focused ultrasound ablation method that ablates tissue through the generation of acoustic cavitation at the transducer focus [15]–[19]. Histotripsy uses microsecond long, high-pressure pulses to generate a histotripsy bubble cloud inside of the targeted tissue [20]–[24]. The rapid expansion and collapse of the

cavitation bubbles result in complete disruption of the tissue [25]. As a nonthermal ablation modality, histotripsy has shown the potential to overcome the limitations associated with thermal ablation. For instance, hepatic histotripsy has been shown to produce consistent and complete ablation in highly vascular regions of the liver [18], [26]. Histotripsy has also shown the ability to preserve vital structures, such as major vessels, bile ducts, and nerves within the ablation zone [18], [27]. Preclinical *in vivo* studies of hepatic histotripsy in healthy porcine and rodent models have demonstrated that histotripsy can generate clinically relevant ablation zones with sharp boundaries (<1 mm) between treated and healthy liver tissue [15], [17], [18], [26], [27]. Additional studies have shown the *in vivo* feasibility of treating HCC tumors in rodent models using histotripsy [19], [28]. Based on these successful preclinical studies, a Phase I clinical trial in patients with liver cancer was recently conducted to demonstrate the feasibility of hepatic histotripsy [16]. Together, these studies have established the feasibility and overall safety profile of hepatic histotripsy.

Although one patient with CC was reportedly treated as part of the clinical trial mentioned above, there have been limited studies investigating the potential of histotripsy for treating CC tumors. CC tumors pose a unique challenge for ablation modalities due to their common location near vital critical structures [29]. The vessel and duct sparing features of hepatic histotripsy are promising for the treatment of CC located near these structures. However, given that prior studies showing fibrous tissues with higher stiffness and mechanical strength are more resistant to histotripsy, it is also expected that CC tumors may pose a unique challenge for histotripsy. This hypothesis is based on the CC tumor's dense desmoplastic fibrotic composition and higher stiffness that have been reported previously [24], [30], [31]. For instance, prior work has found the average Young's modulus of CC tumors to be 56.9 ± 25.6 kPa, which was significantly higher than HCC (14.86 ± 10.0 kPa) and LM (28.8 ± 16.0 kPa) tumors [32]. Given these mechanical profiles, we hypothesize that histotripsy will require higher treatment doses to ablate CC tumors compared to LM and HCC.

In this study, we investigate the feasibility of using histotripsy for the treatment of CC tumors. To test histotripsy for CC ablation, this study was split into two parts. In part one, we investigate the *in vivo* feasibility of histotripsy CC ablation in a subcutaneous patient-derived xenograft (PDX) CC tumor model. In part two, we perform a comparative dosimetry study for treating *ex vivo* human HCC, LM, and CC tumors with histotripsy to determine the differences in treatment dose requirements for ablating each tumor type with histotripsy.

II. PROCEDURES

A. Histotripsy Systems

Two separate histotripsy systems were used in this study for the small animal and large animal *in vivo* histotripsy studies. Small animal *in vivo* experiments were conducted using a custom eight-element 1-MHz histotripsy transducer with a geometric focal distance of 36 mm, an aperture size of 52.7 mm, and an f-number of 0.68 [see Fig. 1(b)]. The transducer was driven via a custom high-voltage pulser designed to generate short therapy pulses of less than two cycles controlled by a field-programmable gate array (FPGA) board (Altera DE0-Nano Terasic Technology, Dover, DE, USA) programed for histotripsy therapy pulsing.

The transducer was positioned in a tank of degassed water beneath a custom-designed mouse surgical stage (see Fig. 1) and attached to a computer-guided 3-D positioning system with a 0.05-mm motor resolution to control the automated volumetric treatments. A linear ultrasound imaging probe with a frequency range of 10–18 MHz (L18-10L30H-4, Telemed, Lithuania, Europe) was coaxially aligned inside the transducer for treatment guidance and monitoring [19], [28]. The transducer was powered by a high voltage dc power supply (GENH750W, TDK-Lambda), and the system was controlled using a custom user interface operated through MATLAB (MathWorks).

For the *ex vivo* experiments, histotripsy was applied using a 36-element 700-kHz clinical histotripsy transducer and associated driving systems (HistoSonics, Inc.) that was previously used in a human clinical trial for the treatment of benign prostatic hyperplasia [33] and multiple previous preclinical studies [24], [34]. This system is the same frequency as the clinical histotripsy system used in the recent Phase I human liver cancer trial [16] and was, thus, chosen for this study. The transducer consists of a concave circular aperture with a small inlet on the perimeter to allow for histotripsy treatments to be guided by a transrectal imaging probe (note that this imaging probe was not used in this study [24], [34]; the transducer has a geometric focal distance of 11 cm and full-width half-maximum (FWHM) dimensions at a geometric focus of 4.0, 4.0, and 15.0 mm in the transverse, elevational, and axial dimensions, respectively. The transducer was powered by a high-voltage dc power supply (GENH750W, TDK-Lambda), and the system was controlled using a custom user interface called the Histotripsy Service Tool (HistoSonics, Inc.) to produce five-cycle histotripsy pulses [24], [35].

B. Pressure Calibration

Focal pressure waveforms for the 1-MHz and 700-kHz transducers were measured by a high sensitivity rod hydrophone (HNR-0500, Onda Corporation, Sunnyvale, CA, USA) and a custom-built fiber optic probe hydrophone (FOPH) [36], [37] in degassed water at the focal point of each transducer. Focal pressures were directly measured with the FOPH up to a peak negative pressure (p-) of ~16 MPa for the 700-kHz transducer and ~20 MPa for the 1-MHz transducer. Pressures were not directly measured beyond these limits due to cavitation on the tip of the hydrophone probe. Waveforms at higher p- were estimated using the linear summation of the pressure waveforms directly measured from four subapertures of the array for the 700-kHz transducer and two subapertures for the 1-MHz transducer. This method showed close agreement between directly measured pressures and the cavitation threshold seen experimentally [38]. All waveforms were measured using a Tektronix TBS2000 series oscilloscope at a sample rate of 500 MS/s, with the waveforms averaged over 128 pulses and recorded in MATLAB.

C. Histotripsy in Vivo CC Ablation Procedure

The feasibility of histotripsy for CC tumor ablation was tested *in vivo* using a PDX CC mouse model. Twelve female NSG mice with subcutaneous flank PDX CC tumors were ordered from and prepared by Jackson Laboratory (Bar Harbor, ME, USA). Through a process previously described for pancreatic PDX tumors [39], a human CC tumor was collected from a patient and propagated as a heterogeneous tumor in immune-compromised

NSG mice. Once received, animals were monitored three times weekly under Virginia Tech IACUC protocols. At each check, general health was monitored, and the tumor diameter was determined by taking two perpendicular measurements, one of which was the widest point of the tumor. Single tumor diameter was calculated as the square root of the product of the two measurements. The mice underwent histotripsy treatment when their tumors reach the targeted treatment size of ~5-mm diameter. Before treatment, fur was removed over the tumor and the surrounding area by applying Nair (Naircare, Ewing, NJ, USA) for 1–2 min and removed by wiping off with a wet paper towel. For treatment, mice were anesthetized with isoflurane (1.5-L/min oxygen flow rate with 1.0%−2.5% isoflurane) and placed prone on the subject stage (see Fig. 1) with their tumor submerged underwater. Animals' respiratory rate and rhythm were monitored during treatment by trained personnel.

The overall setup for the *in vivo* treatment is illustrated in Fig. 1. This custom system, which has been used in previous small animal *in vivo* histotripsy studies [17], [19], [28], consists of the 1-MHz histotripsy transducer with coaxially aligned ultrasound imaging positioned vertically underneath a small animal surgical stage inside a heated water tank that allows for acoustic coupling. A second water tank is connected to this primary tank to circulate warmed, degassed water at a constant temperature throughout the procedures. Before treatment, the water tanks were filled with water and degassed for approximately 1 h. A water heater was used to maintain the water temperature at 37 °C + 4 °C throughout the treatment. A small animal platform containing a hole in the center was located on top of the tank for an anesthetized mouse to be placed with the mouse's flank containing the tumor submerged in the water at the transducer focus. The transducer and a coaxially aligned imaging probe were connected to a 3-D motorized positioning system that was used to apply an automated volumetric ablation to a targeted volume within the tumor. This custom volumetric ablation system was designed to allow the user to outline the desired tumor and treatment regions before starting treatment. The treatment volume was then divided into a 3-D grid of points, and histotripsy was raster-scanned through a series of treatment points spaced by 1.5 mm in the axial direction and 0.5 mm in the lateral directions. While all the tumors were treated at different sizes due to delayed growth and planning in between treatments, the goal was to treat tumors when they averaged 5 mm in diameter. For a 5-mm-diameter tumor, the spacing resulted in treatment with 1382 treatment points, a dwell time of 2 s, and a 46-min treatment. This treatment spacing was determined based on preliminary experiments to ensure overlap between adjacent bubble clouds. Three separate treatment doses of 250, 500, and 1000 pulses/point were tested to determine the feasibility of histotripsy for treating CC tumors *in vivo*, with the results compared to an untreated group ($n = 3$/group). Treatment dose was determined based on prior small animal studies that utilized 50–500 pulses to treat healthy liver and HCC tumors in addition to the hypothesis that CC tumors would require a high dose given their higher mechanical strength [17], [19], [28].

D. Human Liver Tumor Specimens for Ex Vivo Treatments

Liver tumor specimens were obtained by consent from patients with resectable HCC, colorectal LM (CLM), or CC tumors in accordance with the Institutional IRB approved protocol (Carilion Clinic, Roanoke Memorial Hospital, Roanoke, VA, USA). Patients with

either biopsy-proven or radiologically diagnosed liver tumors were consented and enrolled in the study. At the time of resection, the resected tissues were sent fresh to pathology for processing, and any tissue above what was needed for clinical evaluation was donated to this study. When possible, surrounding liver parenchyma (LP) was also collected and used to evaluate the histotripsy doses for ablating LP tissue within the surgical margin. After harvesting, the tumor specimens were placed in a 0.9% degassed saline solution. Before treatment, samples were degassed inside a saline solution in a vacuum chamber (20–25 kPa) for 30–60 min. After degassing, the harvested tumor samples were sectioned into 0.5–1-cm^3 samples and embedded in 7.5% degassed gelatin (porcine gelatin, Millipore Sigma) tissue phantoms for treatment [see Fig. 2(c)]. Gel phantoms containing the embedded tumor samples were then refrigerated for up to 8 h, with all specimens treated within 24 h of the initial harvest.

E. Histotripsy Ex Vivo Ablation Procedure

The treatment doses that required ablating HCC, CLM, and CC tumors were investigated by histotripsy applying to the excised tissue samples embedded inside gelatin phantoms, as described above (see Fig. 2). For all experiments, the 700-kHz histotripsy therapy transducer was used to apply five-cycle pulses to the center of the tissue samples at a PRF of 500 Hz. These parameters closely match the histotripsy parameters used in previous shock-scattering histotripsy liver ablation studies [15], [16], [18], [27]. For each treatment, tissue samples embedded in gelatin were mounted to a motorized 3-D positioning system and aligned to the focus of the therapy transducer (see Fig. 2). To guide treatments and visualize the histotripsy cavitation bubble cloud in real time, an ultrasound imaging probe (SL18-5, AIXPLORER, SuperSonic Imagine) was mounted perpendicularly to the tissue and aligned to the focal location of the therapy transducer [see Fig. 2(b)]. The focus of the histotripsy transducer was located and marked on the imaging screen before each experiment by generating a bubble cloud in open water and then marking the location on the imaging screen before aligning the tissue at the focus. Tissue samples were then positioned such that the focal point of the transducer was located at the desired location within the tissue.

The pressure required to generate histotripsy cavitation inside each tissue sample was measured by gradually increasing the pressure at the focus until a cavitation cloud was identified on US imaging. The pressure at which a consistent histotripsy bubble cloud was generated inside each tissue sample was recorded as the cavitation cloud threshold before conducting volumetric ablation experiments in each sample.

Histotripsy was applied to the targeted volume at a pressure level chosen to be ~30% above the cavitation threshold, which corresponded to treatments with applied p-between 19 and 33 MPa, depending upon the sample. Volumetric treatments were then applied automatically to a predetermined 3-D grid of equally spaced treatment points, with 2.5-mm spacing in the axial direction and 1-mm spacing in the later directions to ensure overlap between adjacent bubble clouds. For each experiment, this grid of points was treated with histotripsy by mechanically scanning the therapy focal zone to cover the targeted portion of the tumor sample. The ideal treatment was a 5 mm × 5 mm × 5 mm cube consisting of 75 total points to dwell at. Given that some samples were too small to achieve this with a contained ablation

volume, not all ablations were this large. The desired size for each sample was 15 mm × 15 mm × 15 mm. However, due to the irregular shapes of the tumors and the small size of some samples, this was not always achievable. The smallest sample treated in this study was a CC tumor that was approximately 8 mm × 8 mm × 8 mm, which led to a treatment size of 2.5 mm × 3 mm × 3 mm.

For each tumor type, three to five groups were treated with histotripsy at different doses to characterize the extent of tissue ablation generated at different histotripsy doses (i.e., the number of pulses/point). The number of pulses applied per point ranged from 500 to 2000 pulses/point for HCC and CLM tumors and 1000 to 4000 pulses/point for CC tumors. These treatment doses were chosen based on previous liver histotripsy studies [15], [24], [40], with the higher doses used for CC tumors based upon a combination of previous histotripsy studies on excised tissues [30], the relationship between histotripsy susceptibility and mechanical properties [24], [30], and the literature showing that CC has an increased Young's modulus [32]. In addition to the liver tumor ablation experiments, a separate set of treatments was conducted on LP tissues collected from the surgical margins around the tumors at doses of 250–1500 pulses/point. A sample size of $n = 3$ per tissue type and treatment dose was used for all experiments when possible. However, due to limitations in tissue availability, this sample size could not be achieved for all tissues and all doses. Based on the availability of donated tissue samples, a total of 49 experimental treatments were conducted in this study, including eight HCC tumor samples, 15 CLM tumor samples, 12 CC tumor samples, and nine LP tissue samples. For each tissue, the sample numbers treated per dose are listed in Table I.

F. Histology & Morphological Analysis

After treatment, tissue specimens were visually inspected and fixed in 10% formalin for at least 24 h before sectioning and staining. Given that each treatment was focused on the center portion of the tissue, the central region of each tissue was sectioned into a cassette. Using standard protocols, all tissues were paraffin-embedded and stained using hematoxylin and eosin (H&E), by ViTALS (Virginia Tech Animal Laboratory Services, Blacksburg, VA, USA), to assess for histotripsy damage to the tissue parenchyma and any other changes in structure and density of collagen and other tissue structures within the ablation volume. To determine the estimated extent of tissue ablated within the targeted volume, regions of cellular damage were compared with regions that were outside of the ablation zone. Results were then verified by a veterinary pathologist (SCO) and a human pathologist (DG) to ensure accuracy and avoid biases. Histology images are representative of the samples treated.

III. Results

A. Histotripsy Ablation of Subcutaneous PDX CC Tumors

Well-defined histotripsy bubble clouds were observed at the focal locations in all tumors at the beginning of the treatment [see Fig. 1(b)]. Throughout the automated volumetric treatments, the bubble clouds were continuously observed at the focus as dynamically changing hyperechoic regions within the tissue. After the treatment, histotripsy ablation

zones that matched the regions exposed to the bubble cloud could be visualized on ultrasound imaging at each of the three doses tested, with more clearly defined hypoechoic regions observed on ultrasound imaging as the treatment dose increased from 250 to 1000 pulses/point [see Fig. 3(b)–(d)]. The histological analysis of the ablation zones showed complete ablation (no remaining intact cells) of the CC tumors within the center of the treated region after 250-pulses/point treatments [see Fig. 3(j)]. Similarly, results for the 500- and 1000-pulses/point treatment groups showed complete ablation of the CC tumors inside the treated regions [see Fig. 3(k) and (l)]. The histological analysis also showed more well-defined treatment margins with increasing treatment dose [see Fig. 3(f)–(h)]. More specifically, results from the 250- and 500-pulses/point treatments showed small (<150 μm) regions of disrupted tissue on the margins between ablated and intact tissue that included intact cells within the boundary region [see Fig. 3(f) and (g)]. In contrast, these partially treated boundary regions were not observed for the 1000-pulses/point treatments that contained a well-defined boundary between the completely treated region and the surrounding intact tissue [see Fig. 3(h)].

B. Histotripsy Bubble Cloud Generation in Ex Vivo Tissue Specimens

The p-required to generate histotripsy bubble clouds inside each of the different tissue types using the 700-kHz clinical histotripsy transducer was measured to be 22.2 ± 1.2, 17.7 ± 3.1, 16.5 ± 2.6, and $20.6 + 4.6$ MPa for HCC, CLM, CC, and LP samples, respectively. In general, the bubble clouds in all tissue types showed typical histotripsy features with a dense dynamically changing hyperechoic bubble cloud observed within or near the focal region of the transducer, as visualized on US imaging. During volumetric ablation experiments, the hyperechoic bubble clouds were maintained throughout the treatments in all tissue experiments. In some samples, particularly, samples smaller than the desired 15 mm × 15 mm × 15 mm dimensions, the cavitation bubble clouds formed at the interface of the gelatin phantom and the tissue including instances of both prefocal and postfocal cavitation clouds. These effects were observed more often in the CLM and CC samples. In cases in which prefocal cavitation was noted during the initial bubble cloud generation, the treatment zone was adjusted to a deeper in the sample when possible and the volumetric treatments were only included as part of this study for samples in which a focal bubble cloud remained present for the duration of the treatment.

C. Histotripsy Ablation of Ex Vivo HCC Specimens

For HCC samples treated with 500 or more pulses/point [see Fig. 4(b)–(d) and (f) and (h)], histotripsy resulted in complete ablation of the targeted tumor volume with no notable regions of intact cells remaining inside the ablated area. There was tumor necrosis characterized by remaining cell nuclei and other subcellular tissue debris inside the treated regions on these samples, with the number of these nuclei reduced in concentration for the higher treatment doses. At 1000 pulses/point or more, there was a complete loss of cellular structures characterized as tissue ablated to amorphous debris.

D. Histotripsy Ablation of Ex Vivo CLM Specimens

The histological analysis demonstrated partial tumor ablation for CLM samples treated with 500 pulses/point, with more than 75% of cells within the treated region remaining

after treatment [see Fig. 5(b) and (g)]. Small, sporadic foci of ablation were observed inside of these samples, with the majority of the treatment volume remaining intact. For 1000-pulses/point CLM samples, a larger portion of the tumor samples was observed to be ablated after treatment with ~25%–75% of the targeted region containing viable tumor tissue after histotripsy [see Fig. 5(c) and (h)]. At the higher treatment doses of 1500 and 2000 pulses/point, histotripsy was observed to generate significantly more tissue damage with complete ablation of the targeted tumor regions observed in some of the samples at both doses [see Fig. 5(d), (e), (i), and (j)]. However, results showed a large amount of variability in the extent of ablation among treatments within each group, with some samples showing only partial tumor ablation. More specifically, the number of viable cells remaining after treatment ranged from <5% (complete ablation) to ~25% in each group, with complete ablation achieved in two of the three samples at 1500 pulses/point and one of the two samples tested at 2000 pulses/point. It was noted that the tissues that did not show complete ablation within these groups appeared to contain more glandular structures and, thus, were well-differentiated. Less differentiated tumors with the poor cellular organization had greater ablation. Similarly, the histological analysis showed the CLM tumors tested in this study exhibited varying degrees of fibrosis within the tumor. Partial ablations were most often exhibited by CLM tumors with a robust, desmoplastic (or fibrous) response. For example, for the 1000-pulses/point samples shown in Fig. 5, the ablated regions of the tumor are found sporadically within the more fibrous regions of the tissue showing loss of cellular detail but still maintaining the fibrotic tissue architecture [see Fig. 5(c) and (h)]. In contrast, the extent of ablation was significantly higher within the less fibrotic regions of these tumors. This effect can be seen in the example 2000-pulses/point image shown in Fig. 5, in which large regions of the tissue were fully ablated, with the remaining tissue lacking cellular detail but with a few nuclei corresponding to the more fibrotic portions of the tumor.

E. Histotripsy Ablation of Ex Vivo CC Specimens

The histological analysis demonstrated partial tumor ablation for CC samples treated with 1000 pulses/point, with sporadic foci of ablated tumor observed throughout the treated volume with interspersed regions of intact tumor [see Fig. 6(b) and (g)]. Results for the 1500- and 2000-pulses/point treatments showed similar results with larger regions of complete loss of cellular detail, supporting a completely ablated portion of the tumor in these samples (see Fig. 6) compared to the 1000-pulses/point group [see Fig. 6(b) and (g)]. For example, the 2000-pulses/point sample shown in Fig. 6 has two visible regions of the tumor, which were not fully ablated; both of them correspond to more fibrotic regions of the tissue. In contrast, the fully ablated regions within this sample appear to correspond to less dense and less fibrotic regions of the tumor. At the highest treatment dose of 4000 pulses/point, histotripsy again resulted in a similar result with only partial ablation generating within each of the CC tumors and ~50%–75% of the cells showing viable nuclei but with loss of cytoplasmic detail within the ablation region remaining after treatment [see Fig. 6(e) and (j)]. In these samples, the sporadic foci of ablation again appeared to be located in the regions of the tissue low in fibrosis (see Fig. 6). Looking at these foci under higher magnification, the tissue within these ablated regions showed complete ablation with no remaining viable cells. In contrast, the less ablated regions of the CC tumors were highly more fibrotic with >75%–90% of viable cells remaining after treatment, as shown in Fig.

S1 in the Supplementary Material. Finally, it is important to note that a high amount of variability in the extent of ablation was observed among treatments within each group. Several of the treatments resulted in >75% ablation (<25% of viable cells remaining) at dosing regimens of 1000, 1500, 2000, and 4000 pulses/point, whereas other treatments resulted in <25% ablation with the majority of the targeted region remaining intact after treatment.

F. Histotripsy Ablation of Ex Vivo LP Specimens

Part of the surrounding LP was excised in addition to the tumor for six patients enrolled in this study. Four patients had hepatic steatosis as identified by abdominal imaging. One patient had hemochromatosis in addition to steatosis, one was hepatitis C positive with fibrosis, and another patient had no identifiable liver disease. These samples were divided based on the presence of steatosis. On histology, tissues from patients with hepatic steatosis were readily apparent based on the presence of macrovesicular fat globules within the tissues. For nonsteatotic samples, a sample size of $n = 1$ was conducted at 250, 500, and 1000 pulses/point. Steatotic samples were treated at $n = 2$ at 250 pulses/point, $n = 3$ for 500 pulses/point, and $n = 1$ for 1000 pulses/point. Complete ablation was formed within the tissues that did not have hepatic steatosis even at doses as low as 250 pulses/point (see Fig. 7). In comparison, tissues with hepatic steatosis were noted to have sporadic foci of ablations at 250 pulses/point with more complete ablation generated at the higher doses. For instance, only a few remaining viable cells were visible inside the ablation zone after 500 pulses/point, and complete ablation of the treated region was observed after 1000 pulses/ point (see Fig. 8).

IV. Discussion

To study the potential of histotripsy for CC tumor ablation, this work first investigated the *in vivo* feasibility of histotripsy CC ablation in a PDX mouse model, with results showing that histotripsy could achieve precise and complete ablation within the targeted region of the tumor. The treatment doses used to treat the CC tumors in this study were higher than those reported previously for xenografted HCC tumors [19]. Given the known correlation between tissue mechanical properties and susceptibility to histotripsy, we hypothesize that this difference is likely due to the higher mechanical strength of CC tumors [24], [30], [31]. Overall, the results from this *in vivo* feasibility study suggest that histotripsy will be capable of treating CC tumors if the proper treatment dose is applied.

In the second part of this study, the effectiveness of histotripsy for ablating CC tumors was compared to HCC and CLM tumors, as well as LP tissue from the surgical margin, in *ex vivo* experiments using human tumor specimens. Overall, the results of these experiments help to demonstrate the histotripsy dosimetry metrics for treating CC in comparison to HCC and CLM liver tumors. More specifically, the results showed that both the CC and CLM tumors required higher treatment doses before tissue ablation was observed in comparison to the softer HCC and LP samples that showed complete tumor ablation at lower treatment doses. These findings match prior studies that have shown fibrous tissues, which have been reported to have higher mechanical strength, are more resistant to histotripsy, and,

therefore, require higher treatment doses [24], [30], [31]. Results from HCC treatments demonstrated that HCC can be completely ablated with histotripsy of fewer than 500 pulses/point, agreeing with previous reports that histotripsy has the potential for rapid, precise, and complete ablation of primary liver tumors. Since CLM tumors are stiffer than HCC tumors [30], [24], we hypothesized that higher treatment doses would be required for generating ablation in these samples. Results supported this hypothesis, showing that histotripsy was able to achieve only small regions of partial ablation for 500 pulses/point. At higher treatment doses of 1500 and 2000 pulses/point, nearly complete or complete ablation was observed in several CLM samples, with the only untreated regions corresponding to highly fibrous regions within the tumor sample.

For *ex vivo* experiments with CC tumors, the trends were similar to those observed for CLM with higher doses again being needed to generate ablation in the CC tumors. Even at the highest doses treated in this study (4000 pulses/point), there were no cases in which we observed complete ablation of the entire treatment volume within the CC tumors, suggesting that higher doses will be needed to achieve full ablation of these highly fibrous CC tumors. This finding appeared to be at least partially due to the large variation in tissue composition between samples and the heterogeneity of the tissue within a given sample (see Fig. S1 in the Supplementary Material). Partial ablations were more pronounced in the CC and CLM tumor samples. We hypothesize that this is due to the higher mechanical strength and the more fibrous nature of these tumors.

Although complete ablation was not generated in the *ex vivo* CC tumors, significant ablation was observed for treatments at the two highest doses tested, with nearly 75% of the treated volume ablated after 2000 and 4000 pulses/point. Overall, these results highlight the need for tumor-specific treatment strategies in future clinical treatments of liver tumors with histotripsy to ensure complete ablation of CLM and CC tumors and more efficient ablation of HCC tumors. For instance, these approaches could include the development of guidelines for the treatment doses (histotripsy pulses/point) needed for treating different tumor types and the development of optimized pulsing parameters although further work would be needed in order to investigate this possibility. In addition, improved real-time feedback methods could be utilized to ensure complete therapeutic ablation of specific tumors, such as those previously developed using bubble-induced color doppler feedback [41], [42] or cavitation detection [43].

In addition to the differences in ablation observed between tumor types, another important observation from this study was the variability in ablation between samples of a given tumor type. This result was possibly due in part to variations in the tissue composition, mainly fibrotic deposits, between any two tumors of the same type and the heterogeneity of the tissue within a single tumor. This effect would explain why the more uniform and softer HCC samples consistently resulted in complete ablation at lower treatment doses compared to more variable results and less complete ablation observed in the more heterogeneous and fibrous CLM and CC tumors. Looking at the regions of partial ablation in these samples, results showed that the foci of ablation interspersed within regions that were not ablated corresponded to the areas with less fibrosis. This result suggests that there is a need for ensuring that histotripsy treatment doses are either optimized for each patient based on

pretreatment assessments of the tumor composition and mechanical characters, such as through MRI or ultrasound elastography. Alternatively, a sufficient treatment dose could be identified based on the most fibrous tumors within each type based upon historically determined mechanical properties. For example, it is possible that the different subtypes of intrahepatic CC (mass-forming, periductal, and intraductal) may respond differently to histotripsy both in the required treatment dose and the efficacy of histotripsy for achieving the desired clinical outcome. Future work should explore this possibility in order to establish the optimal role of histotripsy for the treatment of each subtype of intrahepatic CC, as well as extrahepatic CC, and determine if tumor type-specific treatment methods are required.

However, although we believe that the variations in tissue composition are likely to explain some of the variability in our *ex vivo* tissue experiments and should be considered in future clinical histotripsy treatments, it is also important to note that these findings could also be due to the limitations of our tissue collection methods in this study. Unfortunately, due to the requirements of the clinical pathologists before tissue collection, the samples collected for this study were often smaller than the desired size for performing optimal *ex vivo* histotripsy experiments. In these smaller samples, prefocal bubble clouds were more often observed on the tissue-gel interface especially in the more fibrous CLM and CC tumors, preventing a more uniform histotripsy treatment from being applied to the tissue volume and likely contributing to some of the variable ablation results observed in those tissues. These effects are not expected to occur *in vivo* where much larger tumors that are surrounded by adjacent LP will be treated with histotripsy, therefore minimizing the risk of prefocal cavitation that causes inconsistent tumor ablation.

Another observation from the *ex vivo* experiments conducted in this work was the finding that nonsteatotic LP was readily ablated with histotripsy, similar to HCC samples, whereas higher treatment doses were required to ablate steatotic LP samples. This finding is important for future liver cancer treatments with histotripsy since it is a standard clinical practice to ablate a margin of the surrounding liver around the tumor to destroy all microscopic foci of tumor cells that might be within these regions. The finding that the LP surrounding tumors in patients with hepatic steatosis, or fatty liver, required higher treatment doses compared to those without this disease, should be noted in future studies optimizing treatment parameters for hepatic histotripsy. It is also possible that fatty pockets dispersed throughout the liver could contribute to more diffuse or prefocal cavitation. This effect would make sense since previous work has shown a significantly lower cavitation threshold for fat compared to water-based parenchymal tissues [20], [21]. However, since no consistent differences in cavitation were observed between the steatotic and nonsteatotic LP samples treated in this study, further work remains needed to investigate the role that fat deposits play in hepatic histotripsy and whether any differences in the cavitation threshold can cause variation in ablation completeness similar to what has been observed for differences in tissue fibrosis.

V. Conclusion

This study tested the potential of histotripsy for the treatment of CC tumors for the first time, with results suggesting that histotripsy has the potential to be used as a noninvasive

ablation method for the treatment of CC. Results from the *in vivo* experiments demonstrated that histotripsy could generate precise and complete ablation of CC tumors in a PDX CC mouse model. In the second part of this work, which compared the histotripsy treatment dose required to ablate different types of liver tumors, results showed that CC and CLM tumors required significantly higher doses than HCC tumors. These findings highlight the need for tumor-specific treatment strategies for future histotripsy liver cancer procedures to ensure that more fibrous tumor types, as well as more fibrous regions within a tumor, are completely ablated during histotripsy. Overall, the findings of this study support further investigation of histotripsy for the treatment of CC in addition to HCC and CLM.

Supplementary Material

Refer to Web version on PubMed Central for supplementary material.

Acknowledgment

Biographies

Alissa Hendricks-Wenger received the B.S. degree in bioengineering from the University of Texas at Arlington, Arlington, TX, USA, in 2016, and the Ph.D. degree in translational biology, medicine and health from Virginia Tech, Blacksburg, VA, USA, in 2021. She is currently pursuing the D.O. degree with the Lincoln Memorial University-Debusk College of Osteopathic Medicine, Knoxville, TN, USA.

Her current research interests include ultrasound for noninvasive tissue ablation, cancer, tissue engineering, and cancer immunology.
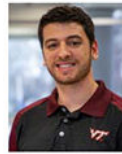

Peter Weber received the B.S. degree in nanomedicine engineering from the University of Virginia, Charlottesville, VA, USA, in 2014, and the M.D. degree from the Virginia Tech Carilion School of Medicine, Roanoke, VA, USA, in 2021.

Alex Simon received the B.S. degree in engineering science and mechanics from Virginia Tech, Blacksburg, VA, USA, in 2019, where he is currently pursuing the Ph.D. degree in engineering mechanics.

His current research interests include focused ultrasound for noninvasive tissue ablation and acoustic cavitation.

Sofie Saunier received the B.S. degree in biological systems engineering from Virginia Tech, Blacksburg, VA, USA, in 2019, where she is currently pursuing the M.S. degree in biomedical engineering.

Sheryl Coutermarsh-Ott received the B.S. degree in biology from the University of Maryland at College Park, College Park, MD, USA, in 2003, and the D.V.M. degree and Ph.D. degree in biomedical and veterinary sciences from the Virginia Maryland College of Veterinary Medicine, Blacksburg, VA, USA, in 2011 and 2017, respectively.

She received specialty training in veterinary anatomic pathology from the University of Georgia College of Veterinary Medicine, Athens, GA, USA, and became achieved board certification in 2014. She is currently an Anatomic Pathologist affiliated with the Virginia Maryland College of Veterinary Medicine and the Virginia Tech Veterinary Teaching Hospital, Blacksburg, VA, USA.

Douglas Grider received the B.S. degree in chemistry from Pacific Lutheran University, Parkland, WA, USA, in 1986, and the M.D. degree from the Uniformed Services University of the Health Sciences, Bethesda, MD, USA, in 1990.

He completed an Anatomic Pathology Fellowship during his last year of residency, and he later went on to complete both a Gastrointestinal and Hepatic Pathology Fellowship and a Dermatopathology Fellowship with the Armed Forces Institute of Pathology, Washington, DC, USA. He is currently the Managing Partner of Dominion Pathology Associates. He

is also an Associate Professor and the Vice Chair with the Department of Basic Science Education, Virginia Tech Carilion School of Medicine, Roanoke, VA, USA.

Joan Vidal-Jové received the M.D. degree in medicine and surgery from the University of Barcelona, Barcelona, Spain, in 1982, the Ph.D. degree in psychology and behavioral sciences from Newport University, Udine, Italy, and the business administration degree from IDEC-Pompeu Fabra, Barcelona.

He was a Surgery Specialist by the Ministry of Health in Spain and the Surgical Oncology Fellowship by the George Washington University, Washington, DC, USA. He is currently the Director of the Comprehensive Tumor Center, Barcelona, and works with the Institute Khuab for Interventional Oncology. He focused Ultrasound HIFU Doctor by the Second University of Chongqing, Chongqing, China. He has authored several publications and conferences.

He is also a Member of the Board of the International Society of Minimal Invasive and Virtual Surgery (ISMIVS), the International Society of Therapeutic Ultrasound (ISTU), and the European Focused Ultrasound Society (EUFUS). He has developed his career in various institutions in USA and Europe, both in the healthcare field, research in industry and public administration. He received awards and research grants in surgical oncology, diagnostic imaging techniques PET, and research in health outcomes. After an educational period in China, he learns the fundamentals of the ablation of tumors by focused ultrasound and returns to lead the first oncological FUSHIFU Unit of his country. Since then, he has performed more than 200 oncological cases with focused ultrasound and lead clinical research, with special attention to pancreatic and liver tumors. He was the PI of the first in human study of histotripsy in liver tumors. Recently, he was the Chairman of the Joint Meeting of the International Society of Therapeutic Ultrasound (ISTU) and the European Focused Ultrasound Society (EUFUS) that was held in Barcelona in 2019.

Irving Coy Allen received the B.S. degree in biology from East Carolina University, Greenville, NC, USA, in 1997, the M.S. degree in biology from the University of North Carolina at Greensboro, Greensboro, NC, USA, in 2000, the Ph.D. degree in genetics and molecular biology from the University of North Carolina at Chapel Hill, Chapel Hill, NC, USA in 2006, and the M.B.A. degree in bioscience management from North Carolina State University at Raleigh, Raleigh, NC, USA, in 2012.

He was a Postdoctoral Fellow with the Lineberger Comprehensive Cancer Center, University of North Carolina at Chapel Hill, from 2007 to 2011. He is currently a Tenured Associate Professor with the Department of Biomedical Sciences and Pathobiology, VA-MD College of Veterinary Medicine, Blacksburg, VA, USA. His current research interests include cancer immunology, animal models of innate immunity, animal models of allergic disease, and host pathogen interactions.

David Luyimbazi received the B.S. degree in molecular biology and biochemistry from Middlebury College, Middlebury, VT, USA, and the M.D. degree from the New York Medical College, Valhalla, NY, USA, in 2005.

He is a board-certified Surgical Oncologist, who completed a General Surgery Residency with the University of Connecticut, Farmington, CT, USA, in 2012. He completed a Fellowship in Complex Surgical Oncology with the City of Hope National Medical Center, Duarte, CA, USA, from 2012 to 2014, He completed a Postdoctoral Surgical Oncology Research Fellowship with the University of Texas MD Anderson Cancer Center, Houston, TX, USA, from 2007 to 2009. He is currently an Attending Surgeon and a Surgical Oncologist with the Carilion Roanoke Memorial Hospital, Roanoke, VA, USA, and an Assistant Professor of surgery with the Virginia Tech Carilion School of Medicine, Roanoke, VA, USA. His clinical focus includes patients who are diagnosed with hepato-pancreato-biliary, peritoneal and foregut malignancies. His interventions include both open and minimally invasive extirpation of organs with tumor, intraperitoneal chemotherapy for peritoneal disease and tumor ablation techniques to treat non-resectable tumors. His past research has included the fundamental study of key signaling pathways that play a role in understanding solid organ tumors. His current focus of interest includes identifying tumor and tissue factors that are predictive of successful uniform ablation of liver tumors and secondly, identifying a reliable way to confirm real-time total intra-operative destruction of tumors post ablation.

Eli Vlaisavljevich is currently an Assistant Professor of biomedical engineering and mechanics with the Virginia Polytechnic Institute and State University, Blacksburg, VA, USA. His research interests include focused ultrasound, non-invasive tissue ablation (HIFU, histotripsy), cavitation physics, nanoparticle-mediated histotripsy (NMH), biomaterials, tissue regeneration, cancer, non-invasive neuromodulation, and clinical translation. Prior to joining Virginia Tech, he conducted his graduate degrees from the Histotripsy Laboratory,

University of Michigan, Ann Arbor, MI, USA, from 2010 to 2015 and then spent two years working with HistoSonics, Ann Arbor, from 2015 to 2017, on the development of histotripsy for the treatment of liver cancer. More information about his research group can be found at https://ultrasound-lab.beam.vt.edu/.

References

[1]. Cancer Facts & Figures 2020, American Cancer Society, Atlanta, GA, USA, 2020.

[2]. Jansen MC, van Hillegersberg R, Chamuleau RA, van Delden OM, Gouma DJ, and van Gulik TM, "Outcome of regional and local ablative therapies for hepatocellular carcinoma: A collective review," Eur. J. Surg. Oncol, vol. 31, no. 4, pp. 331–347, May 2005, doi: 10.1016/j.ejso.2004.10.011. [PubMed: 15837037]

[3]. Rossi L et al. , "Current approach in the treatment of hepatocellular carcinoma," World J. Gastrointestinal Oncol, vol. 2, no. 9, pp. 348–359, Sep. 2010, doi: 10.4251/wjgo.v2.i9.348.

[4]. Nagorney DM, Donohue JH, Farnell MB, Schleck CD, and Ilstrup DM, "Outcomes after curative resections of cholangiocarcinoma," Arch. Surg, vol. 128, no. 8, pp. 871–878, 1993. [PubMed: 8393652]

[5]. Feng K et al. , "A randomized controlled trial of radiofrequency ablation and surgical resection in the treatment of small hepatocellular carcinoma," J. Hepatol, vol. 57, no. 4, pp. 794–802, Oct. 2012, doi: 10.1016/j.jhep.2012.05.007. [PubMed: 22634125]

[6]. Chen MS et al. , "A prospective randomized trial comparing percutaneous local ablative therapy and partial hepatectomy for small hepatocellular carcinoma," Ann. Surg, vol. 243, no. 3, pp. 321–328, Mar. 2006, doi: 10.1097/01.sla.0000201480.65519.b8. [PubMed: 16495695]

[7]. Hammill CW, Billingsley KG, Cassera MA, Wolf RF, Ujiki MB, and Hansen PD, "Outcome after laparoscopic radiofrequency ablation of technically resectable colorectal liver metastases," Ann. Surg. Oncol, vol. 18, no. 7, pp. 1947–1954, Jul. 2011, doi: 10.1245/s10434-010-1535-9. [PubMed: 21399885]

[8]. Otto G, Duber C, Hoppe-Lotichius M, Konig J, Heise M, and Pitton MB, "Radiofrequency ablation as first-line treatment in patients with early colorectal liver metastases amenable to surgery," Ann. Surg, vol. 251, no. 5, pp. 796–803, May 2010, doi: 10.1097/SLA.0b013e3181bc9fae. [PubMed: 19858704]

[9]. Salem R et al. , "Institutional decision to adopt Y90 as primary treatment for hepatocellular carcinoma informed by a 1,000-patient 15-year experience," Hepatology, vol. 68, no. 4, pp. 1429–1440, Dec. 2017, doi: 10.1002/hep.29691.

[10]. Forner A, Llovet JM, and Bruix J, "Hepatocellular carcinoma," Lancet, vol. 379, no. 9822, pp. 1245–1255, Mar. 2012, doi: 10.1016/S0140-6736(11)61347-0. [PubMed: 22353262]

[11]. European Association for the Study, "EASL-EORTC clinical practice guidelines: Management of hepatocellular carcinoma," J. Hepatol, vol. 56, no. 4, pp. 908–943, 2012. [Online]. Available: http://linkinghub.elsevier.com/retrieve/pii/S0168827811008737?showall=true [PubMed: 22424438]

[12]. Gillams A et al. , "Thermal ablation of colorectal liver metastases: A position paper by an international panel of ablation experts, the interventional oncology Sans Frontieres meeting 2013," Eur. Radiol, vol. 25, no. 12, pp. 3438–3454, Dec. 2015, doi: 10.1007/s00330-015-3779-z. [PubMed: 25994193]

[13]. Rozenblum N et al. , "Oncogenesis: An 'off-target' effect of radiofrequency ablation," Radiology, vol. 276, no. 2, pp. 426–432, Aug. 2015, doi: 10.1148/radiol.2015141695. [PubMed: 26203709]

[14]. Sangro B et al. , "Prevention and treatment of complications of selective internal radiation therapy: Expert guidance and systematic review," Hepatology, vol. 66, no. 3, pp. 969–982, Sep. 2017, doi: 10.1002/hep.29207. [PubMed: 28407278]

[15]. Smolock CM, Vlaisavljevich E, Gendron-Fitzpatrick A, and Green C, "Robotically assisted sonic therapy as a non-invasive non-thermal ablation modality: Proof of concept in a porcine liver model," Radiology, vol. 287, no. 2, pp. 485–493, 2018. [PubMed: 29381870]

[16]. Vidal Jove SXJ et al. , "Phase I study of safety and efficacy of hepatic histotripsy: Preliminary results of first in man experience with robotically-assisted sonic therapy," in Proc. Int. Soc. Therapeutic Ultrasound, Barcelona, Spain, 2019, p. 167.

[17]. Vlaisavljevich E et al. , "Non-invasive ultrasound liver ablation using histotripsy: Chronic study in an in vivo rodent model," Ultrasound Med. Biol, vol. 42, no. 8, pp. 1890–1892, Aug. 2016, doi: 10.1016/j.ultrasmedbio.2016.03.018. [PubMed: 27140521]

[18]. Vlaisavljevich E et al. , "Image-guided non-invasive ultrasound liver ablation using histotripsy: Feasibility study in an in vivo porcine model," Ultrasound Med. Biol, vol. 39, no. 8, pp. 1398–1409, Aug. 2013, doi: 10.1016/j.ultrasmedbio.2013.02.005. [PubMed: 23683406]

[19]. Worlikar T et al., "Histotripsy for non-invasive ablation of hepatocellular carcinoma (HCC) tumor in a subcutaneous xenograft murine model," in Proc. 40th Annu. Int. Conf. Eng. Med. Biol. Soc., Jul. 2018, pp. 6064–6067, doi: 10.1109/EMBC.2018.8513650.

[20]. Maxwell AD, Cain CA, Hall TL, Fowlkes JB, and Xu Z, "Probability of cavitation for single ultrasound pulses applied to tissues and tissue-mimicking materials," Ultrasound Med. Biol, vol. 39, no. 3, pp. 449–465, Mar. 2013, doi: 10.1016/j.ultrasmedbio.2012.09.004. [PubMed: 23380152]

[21]. Vlaisavljevich E et al. , "Effects of ultrasound frequency and tissue stiffness on the histotripsy intrinsic threshold for cavitation," Ultrasound Med. Biol, vol. 41, no. 6, pp. 1651–1667, Jun. 2015, doi: 10.1016/j.ultrasmedbio.2015.01.028. [PubMed: 25766571]

[22]. Xu Z et al. , "Controlled ultrasound tissue erosion," IEEE Trans. Ultrason., Ferroelectr., Freq. Control, vol. 51, no. 6, pp. 726–736, Jun. 2004, doi: 10.1109/tuffc.2004.1308731. [PubMed: 15244286]

[23]. Xu Z, Raghavan M, Hall TL, Mycek M, Fowlkes J, and Cain CA, "Evolution of bubble clouds induced by pulsed cavitational ultrasound therapy-histotripsy," IEEE Trans. Ultrason., Ferroelectr., Freq. Control, vol. 55, no. 5, pp. 1122–1132, May 2008. [PubMed: 18519220]

[24]. Vlaisavljevich E, Maxwell A, Warnez M, Johnsen E, Cain CA, and Xu Z, "Histotripsy-induced cavitation cloud initiation thresholds in tissues of different mechanical properties," IEEE Trans. Ultrason., Ferroelectr., Freq. Control, vol. 61, no. 2, pp. 341–352, Feb. 2014, doi: 10.1109/TUFFC.2014.6722618. [PubMed: 24474139]

[25]. Vlaisavljevich E, Maxwell A, Mancia L, Johnsen E, Cain C, and Xu Z, "Visualizing the histotripsy process: Bubble cloud-cancer cell interactions in a tissue-mimicking environment," Ultrasound Med. Biol, vol. 42, no. 10, pp. 2466–2477, Oct. 2016, doi: 10.1016/j.ultrasmedbio.2016.05.018. [PubMed: 27401956]

[26]. Kim Y, Vlaisavljevich E, Owens GS, Allen SP, Cain CA, and Xu Z, "In vivo transcostal histotripsy therapy without aberration correction," Phys. Med. Biol, vol. 59, pp. 2553–2568, Dec. 2014. [PubMed: 24785433]

[27]. Vlaisavljevich E et al. , "Non-invasive liver ablation using histotripsy: Preclinical safety study in an in vivo porcine model," Ultrasound Med. Biol, vol. 43, no. 6, pp. 1237–1251, Jun. 2017, doi: 10.1016/j.ultrasmedbio.2017.01.016. [PubMed: 28318889]

[28]. Qu S et al. , "Non-thermal histotripsy tumor ablation promotes abscopal immune responses that enhance cancer immunotherapy," J. ImmunoTherapy Cancer, vol. 8, 2020, Art. no. e000200, doi: 10.1136/jitc-2019-000200.

[29]. Venkatesh SK et al. , "MR elastography of liver tumors: Preliminary results," Amer. J. Roentgenol, vol. 190, no. 6, pp. 1534–1540, 2008. [PubMed: 18492904]

[30]. Vlaisavljevich E, Kim Y, Owens G, Roberts W, Cain C, and Xu Z, "Effects of tissue mechanical properties on susceptibility to histotripsy-induced tissue damage," Phys. Med. Biol, vol. 59, no. 2, pp. 253–270, Jan. 2014, doi: 10.1088/0031-9155/59/2/253. [PubMed: 24351722]

[31]. Vlaisavljevich E, Xu Z, Arvidson A, Jin L, Roberts W, and Cain C, "Effects of thermal preconditioning on tissue susceptibility to histotripsy," Ultrasound Med. Biol, vol. 41, no. 11, pp. 2938–2954, 2015. [PubMed: 26318560]

[32]. Guibal A et al. , "Evaluation of shearwave elastography for the characterisation of focal liver lesions on ultrasound," Eur. Radiol, vol. 23, no. 4, pp. 1138–1149, 2013. [PubMed: 23160662]

[33]. Schuster TG, Wei JT, Hendlin K, Jahnke R, and Roberts WW, "Histotripsy treatment of benign prostatic enlargement using the Vortx Rx system: Initial human safety and efficacy outcomes," Urology, vol. 114, pp. 184–187, Apr. 2018, doi: 10.1016/j.urology.2017.12.033. [PubMed: 29330000]

[34]. Roberts WW, Teofilovic D, Jahnke RC, Patri J, Risdahl JM, and Bertolina JA, "Histotripsy of the prostate using a commercial system in a canine model," J. Urol, vol. 191, no. 3, pp. 860–865, 2014. [PubMed: 24012583]

[35]. Maxwell AD et al. , "Cavitation clouds created by shock scattering from bubbles during histotripsy," J. Acoust. Soc. Amer, vol. 130, no. 4, pp. 1888–1898, Oct. 2011, doi: 10.1121/1.3625239. [PubMed: 21973343]

[36]. Parsons JE, Cain CA, Abrams GD, and Fowlkes JB, "Pulsed cavitational ultrasound therapy for controlled tissue homogenization," Ultrasound Med. Biol, vol. 32, no. 1, pp. 115–129, Jan. 2006, doi: 10.1016/j.ultrasmedbio.2005.09.005. [PubMed: 16364803]

[37]. Parsons JE, Cain CA, and Fowlkes JB, "Cost-effective assembly of a basic fiber-optic hydrophone for measurement of high-amplitude therapeutic ultrasound fields," J. Acoust. Soc. Amer, vol. 119, no. 3, pp. 1432–1440, Mar. 2006, doi: 10.1121/1.2166708. [PubMed: 16583887]

[38]. Vlaisavljevich E, Gerhardson T, Hall T, and Xu Z, "Effects off number on the histotripsy intrinsic threshold and cavitation bubble cloud behavior," Phys. Med. Biol, vol. 62, no. 4, pp. 1269–1290, Feb. 2017, doi: 10.1088/1361-6560/aa54c7. [PubMed: 27995900]

[39]. Brock RM et al. , "Patient derived xenografts expand human primary pancreatic tumor tissue availability for *ex vivo* irreversible electroporation testing," Frontiers Oncol, vol. 10, p. 843, May 2020.

[40]. Longo KC et al. , "Histotripsy ablations in a porcine liver model: Feasibility of respiratory motion compensation by alteration of the ablation zone prescription shape," CardioVascular Interventional Radiol, vol. 43, pp. 1695–1701, Nov. 2020.

[41]. Macoskey JJ et al. , "Bubble-induced color Doppler feedback correlates with histotripsy-induced destruction of structural components in liver tissue," Ultrasound Med. Biol, vol. 44, no. 3, pp. 602–612, 2018. [PubMed: 29329687]

[42]. Wang T-Y, Hall TL, Xu Z, Fowlkes JB, and Cain CA, "Imaging feedback of histotripsy treatments using ultrasound shear wave elastography," IEEE Trans. Ultrason., Ferroelectr., Freq. Control, vol. 59, no. 6, pp. 1167–1181, Jun. 2012, doi: 10.1109/TUFFC.2012.2307. [PubMed: 22711412]

[43]. Macoskey JJ et al. , "Using the cavitation collapse time to indicate the extent of histotripsy-induced tissue fractionation," Phys. Med. Biol, vol. 63, no. 5, Mar. 2018, Art. no. 055013, doi: 10.1088/1361-6560/aaae3b.
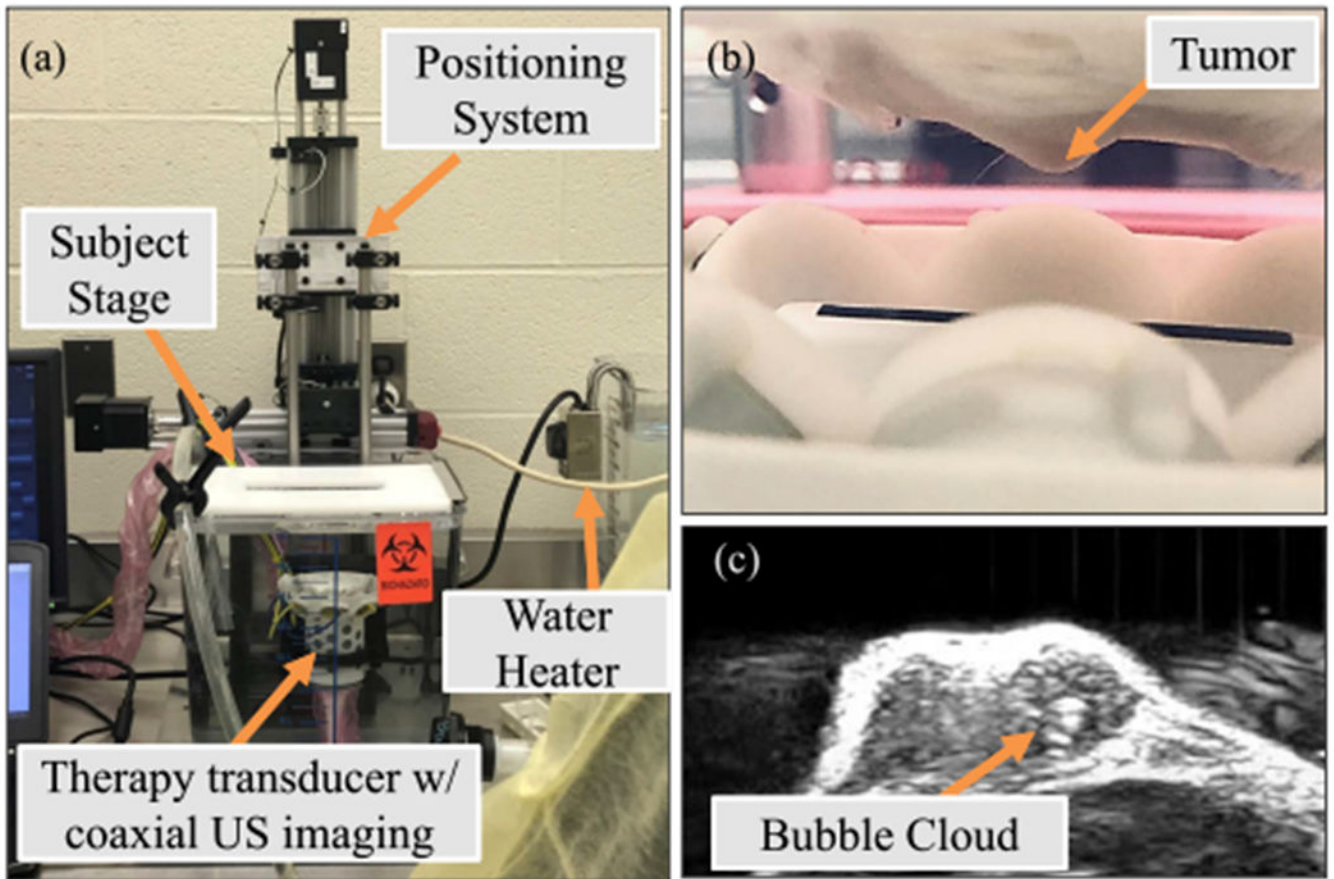
Fig. 1.

In vivo ablation setup. (a) Histotripsy murine experiments were conducted using a custom 1-MHz small animal histotripsy system. (b) Subject's tumors were submerged in degassed water at the transducer focus in order for (c) histotripsy to be applied to the tumor noninvasively guided by real-time ultrasound imaging.
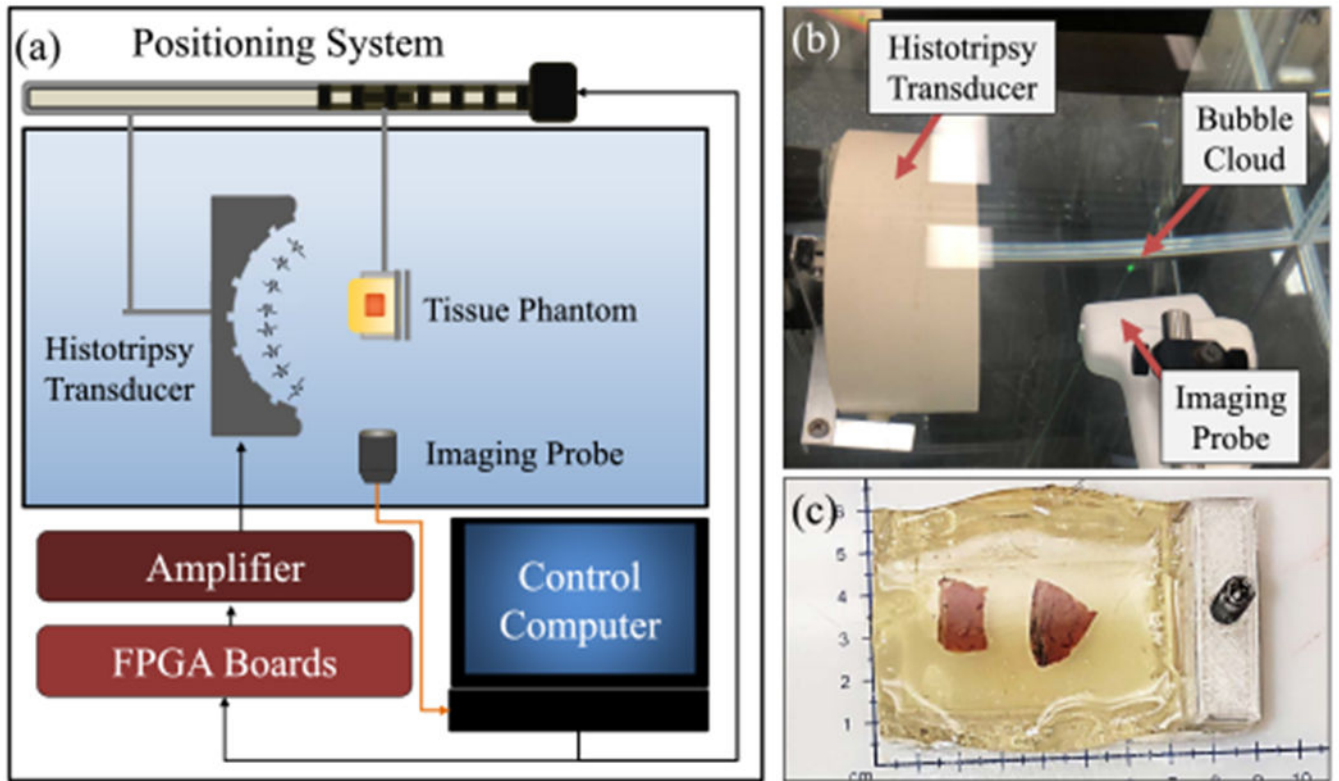
Fig. 2.
Ex vivo tissue ablation setup. (a) and (b) Histotripsy dose experiments were conducted using a 700-kHz transducer with the focus aligned in the center of the targeted tissue, with guidance from ultrasound imaging aligned orthogonally. (c) Tissues were embedded within the center of a gelatin phantom.
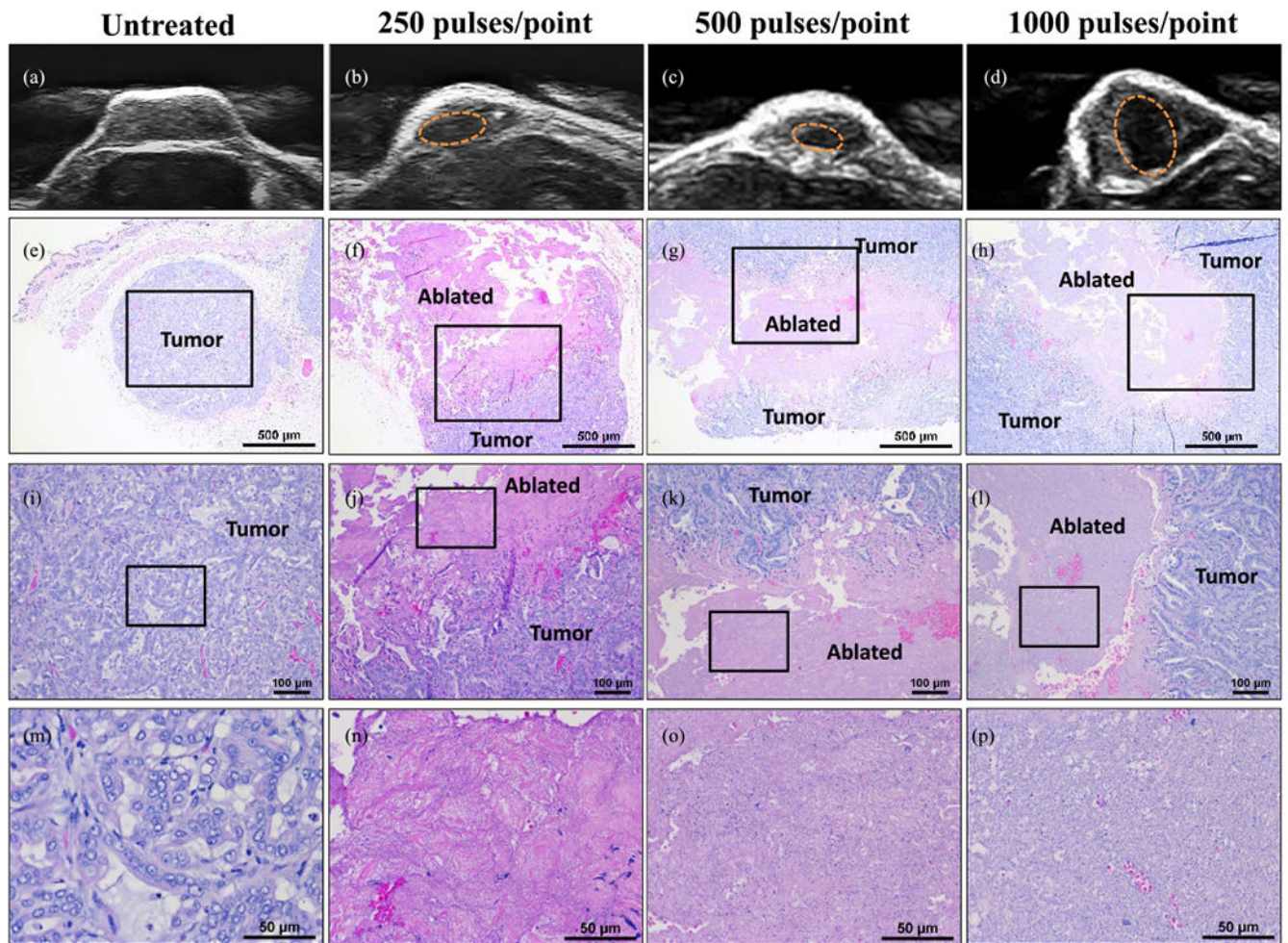
Fig. 3.
Dotted orange circles on US images. (a)–(d) Approximate region of ablation. (e)–(h) Corresponding to ablation region on 4× H&E. (j)–(l) 10x magnification H&E images of control and ablated region. (m)–(p) 40× magnification H&E images show ablation margins. Black boxes indicate area magnified in respective images. Scale bar on (e)–(h) 4× H&E images = 500 μm, (j)–(l) 10× scale bar = 100 μm, and (m)–(p) 40× scale bar = 50 μm.
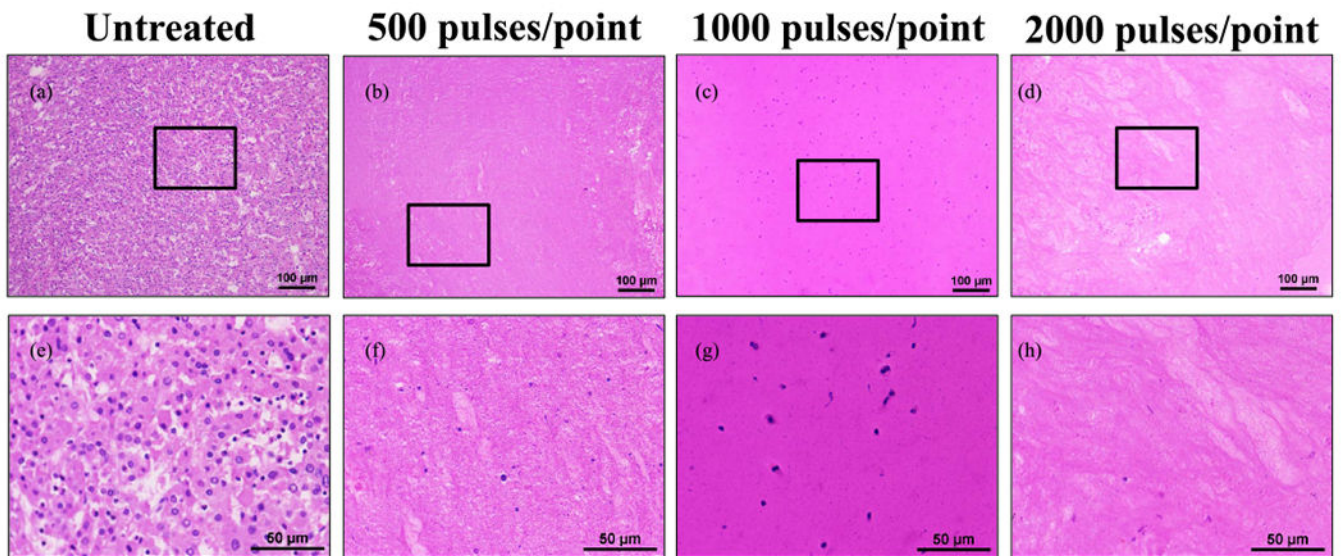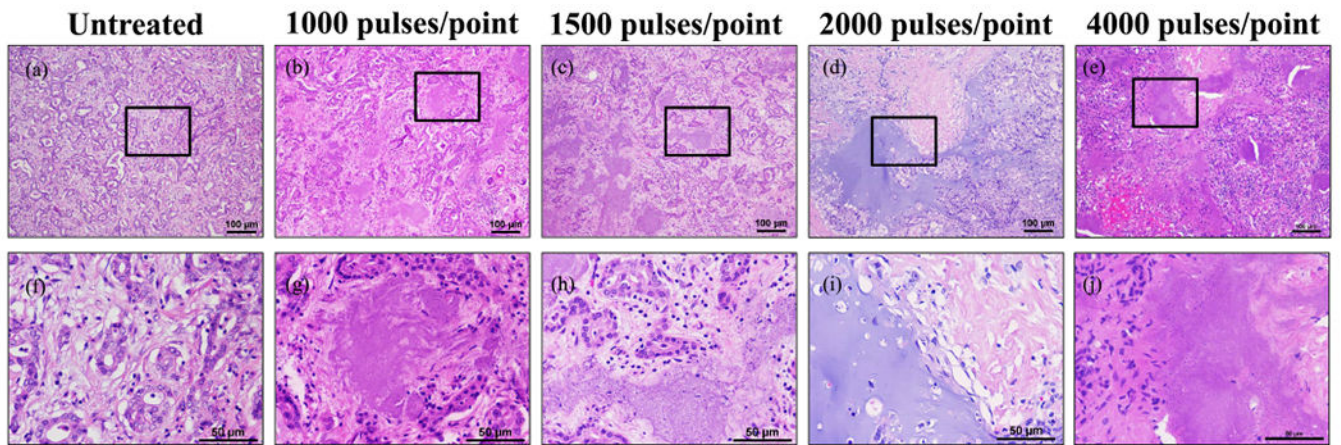
Fig. 4.

Comparison of untreated human HCC tumors with *ex vivo* ablations at 500, 1000, and 2000 pulses/point. (a)–(d) 10× magnification scale bar = 100 μm. (e)–(h) 40× scale bar = 50 μm. Black boxes on 10× images indicate area magnified in respective 40× images. Histology images are representative of the samples treated.
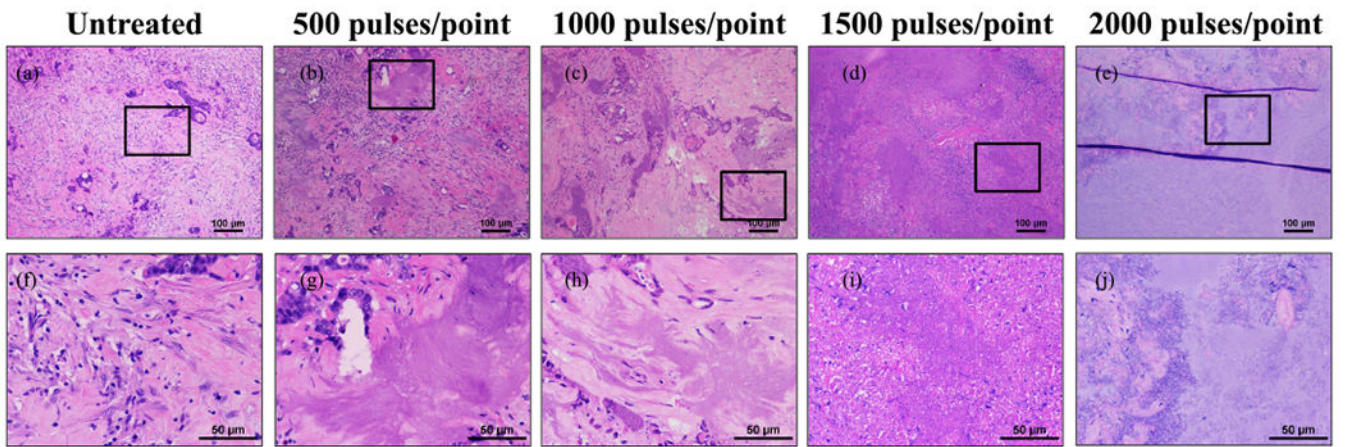
Fig. 5.

Comparison of untreated human CLM tumors with those treated at 500, 1000, 1500, and 2000 pulses/point. (a)–(e) 10× magnification scale bar = 100 μm. (f)–(j) 40× scale bar = 50 μm. Black boxes on 10× images indicate area magnified in respective 40× image. Histology images are representative of the samples treated.

Fig. 6.

Comparison of untreated human CC tumors with those treated at 1000, 1500, 2000, and 4000 pulses/point. (a)–(e) 10× magnification scale bar = 100 μm. (f)–(j) 40× scale bar = 50 μm. Black boxes on 10× images indicate area magnified in respective 40× image. Histology images are representative of the samples treated.
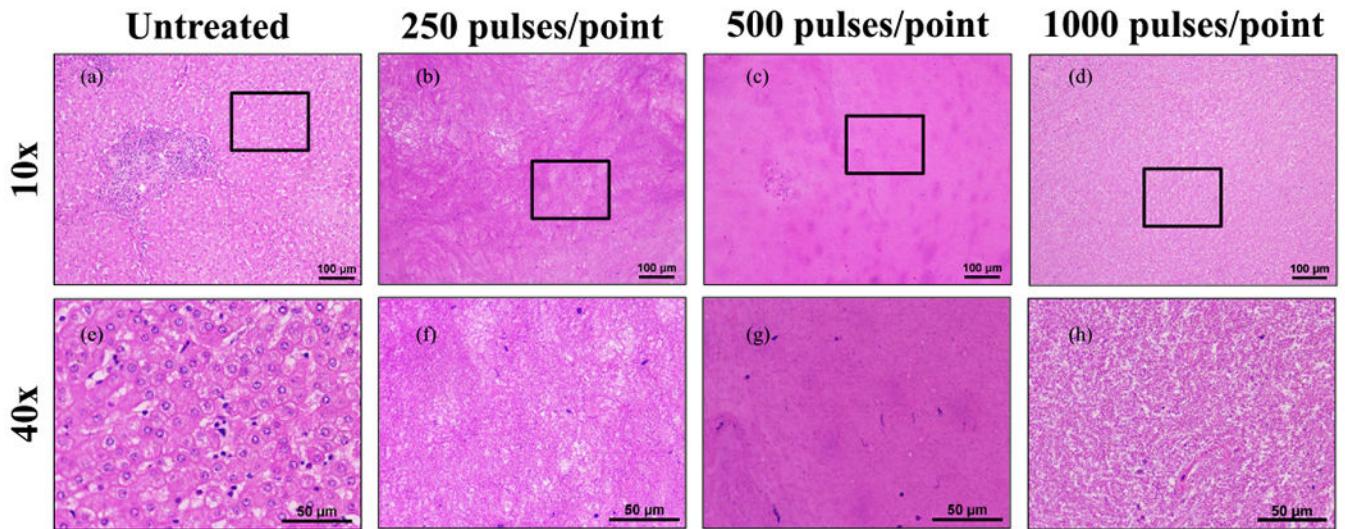
Fig. 7.

Nonsteatotic LP treatment at 250, 500, and 1000 pulses/point demonstrating less uniform ablations. (a)–(d) 10× magnification scale bar = 100 μm. (e)–(h) 40× scale bar = 50 μm. Black boxes on 10× images indicate area magnified in respective 40× images. Histology images are representative of the samples treated.
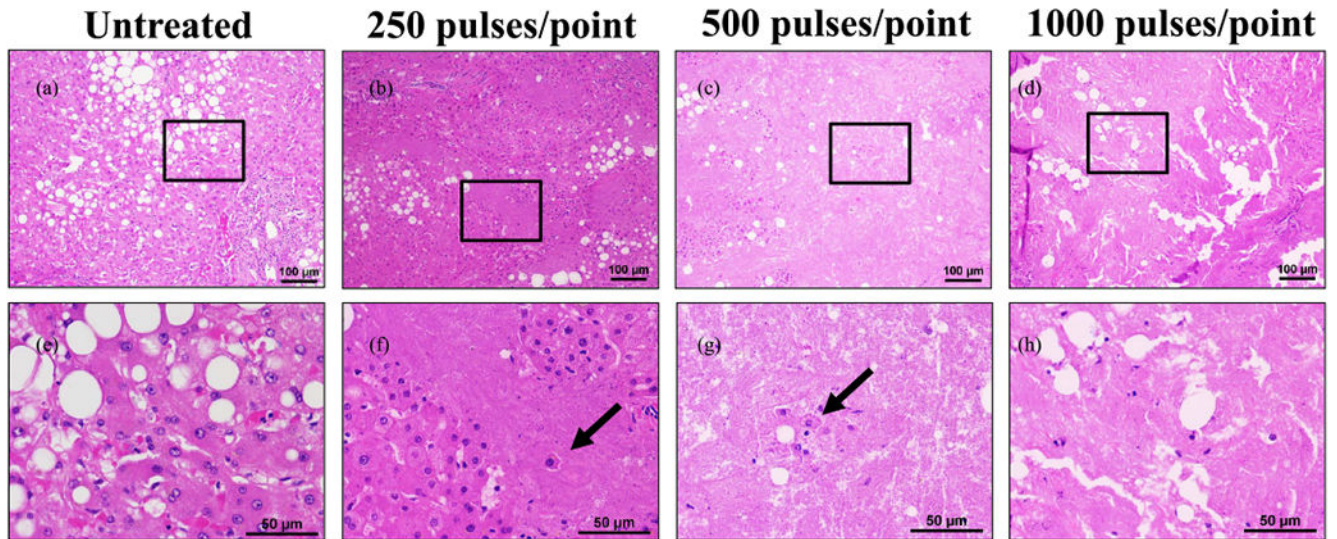
Fig. 8.

Steatotic LP treatment at 250, 500, and 1000 pulses/point demonstrating less uniform ablations. (a)–(d) 10× magnification scale bar = 100 μm. (e)–(h) 40× scale bar = 50 μm. Black boxes on 10× images indicate area magnified in respective 40× images. Arrows indicate example cells within an ablated region that appear to be intact. Histology images are representative of the samples treated.

TABLE I

Ex Vivo Sample Numbers by Tissue Type and Dose

	250	500	1000	1500	2000	4000
HCC		n=2	n=2		n=1	
CLM		n=3	n=3	n=3		
CC			n=3	n=3	n=3	n=2
LP	n=3	n=4	n=2			